An Assessment of Track Fusion Algorithms

A Major Qualifying Project Report:
Submitted to the faculty of

Worcester Polytechnic Institute

In partial fulfillment of the requirements for the

Degree in Bachelor of Science in Mathematical Sciences and Physics

by

Jordan Kovar

Sponsoring Organization:
MIT Lincoln Laboratory

Supervisors:
Drs. David Malling & Lisa Wei

Project Advisors:
Professors Joseph Fehribach & Germano Iannacchione

Contents

List of Figures

Abstract

Radar is a cornerstone of modern intelligence, surveillance and reconnaissance. While radar can determine the location of a target to within a region of space, fundamental uncertainties exist that limit the accuracy of individual radars. A method that is used to reduce these uncertainties is known as data fusion and involves processing the measurements from multiple radars together. One of the main challenges of using data fusion in the field is the difficulty of being able to associate individual detections that correspond to the same target into tracks in real time. Different data fusion algorithms exist to reduce the computation time but the trade-off is lower track accuracy. The goal of the MQP was to quantify these trade-offs for different data fusion algorithms under several scenarios.

In this 1/3 unit extension to the MQP, the radar simulator that was built and used to generate simulated radar data will be examined. Included is a review of the background information needed to understand radar as well as an introduction to the fundamentals of radar, radar detection, and radar tracking. This is proceeded by a full explanation and breakdown of the radar simulator followed by some concluding remarks.

Chapter 1

Introduction

Invented in 1935, the first dedicated radar systems were used by the British to preempt bombing runs by the German Luftwaffe. Ever since then, radar has played a critical role in military surveillance and reconnaissance, in addition to having found numerous non-military applications, ranging from weather forecasting to vehicle collision avoidance systems. Radar, which is an acronym for **RA**dio **D**etection **A**nd **R**anging, uses radio waves to determine the location of targets in its field of view. Early radar systems had poor resolution and were easy to jam, but developments in the 80 years since radar was invented have dramatically improved the resolution and made efforts to jam radar signals far more difficult.

A major advance in the development of radar was the incorporation of the tracker. As radars take discrete measurements of a target at regular intervals, they lack the ability to keep track of targets between those intervals. Further complicating matters is the possibility that there are multiple targets which can make it difficult to determine which blips in the radar correspond to which targets. To be of practical use, it is necessary to take the discrete radar measurements and combine them to form continuous trajectories or tracks, which is where the tracker comes in. A radar tracker takes all of the detections from the radar and forms them into tracks that can be used both to keep track of where a given target has been, as well as predict in the short term where the target is headed.

This paper serves to fulfill the additional 1/3 unit of MQP required for double majors by providing some additional background for the MQP that was completed at MIT Lincoln Laboratory. The goal of the MQP was to assess the relative strengths and weaknesses of different track fusion algorithms

under several different scenarios. This goal was accomplished by creating simulated radar data sets and then using the fusion algorithms on those data sets to draw our various conclusions. This paper will specifically examine the radar simulator portion of the MQP as well as briefly cover the basics of the tracker in the form of the Kalman filter. First, a brief overview of some of the physics-related concepts that pertain to radar will be covered. This will then be followed up by the basics of how radar works, as well as an introduction to radar tracking. Finally, the details of how the radar simulator was constructed will be examined followed by some concluding remarks.

Chapter 2

Background

2.1 Basics of Electromagnetic Radiation

The classical definition of electromagnetic radiation is a self-propagating transverse wave comprised of oscillating orthogonal electric field and magnetic field components. In Figure 2.1, the oscillation of the electric field generates a magnetic field, and in turn, the oscillation of the magnetic field generates an electric field. The mutual generation of the electric and magnetic fields is the origin of the self-propagation of electromagnetic radiation. An important feature of electromagnetic radiation is the wavelength which is also depicted in Figure 2.1. The wavelength, λ, is defined as the distance that the electromagnetic wave travels after one full oscillation of the electric field or magnetic field components. Similarly, the number of oscillations that occur per second is referred to as the frequency, f, of the electromagnetic radiation. In a perfect vacuum, all electromagnetic waves travel at the speed of light, c, which is exactly 299,792,458 m/s. The speed of an electromagnetic wave is related to the wavelength and frequency by the simple equation $c = \lambda f$. Electromagnetic waves have several properties in addition to those mentioned that strongly come into play when working with radar.

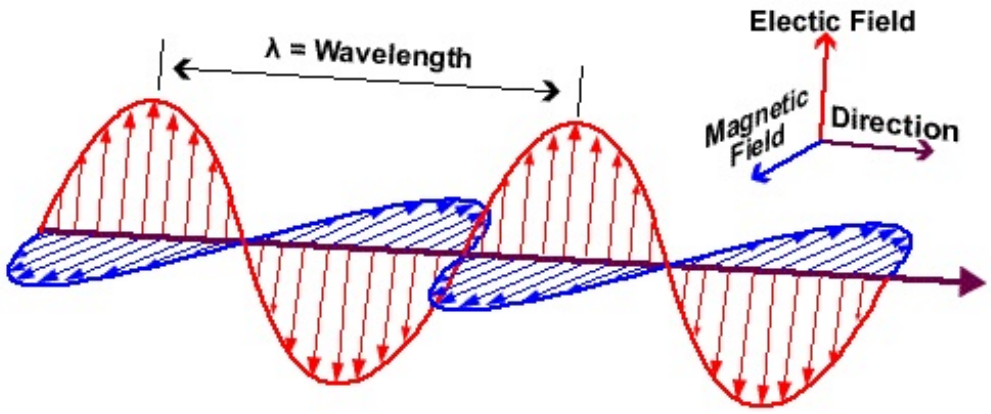

Figure 2.1: Classical electromagnetic radiation is comprised of an electric field component and a magnetic field component [15].

2.1.1 Interference

Interference occurs when two or more electromagnetic waves overlap in some region, resulting in a change in the amplitude of the waves in that region. To understand how this works, consider two identical electromagnetic plane waves with a phase shift between them $A_1(\mathbf{x}, t) = Ae^{i(k\mathbf{x}-\omega t)}$ and $A_2(\mathbf{x}, t) = Ae^{i(k\mathbf{x}-\omega t+\Delta\phi)}$ where $k = 2\pi/\lambda$ is the wavenumber, $\mathbf{x}$ is a position vector, $\omega = 2\pi f$ is the angular frequency of the electromagnetic wave, t is time, and $\Delta\phi$ is the phase shift. The phase shift is the critical quantity when determining how these two waves interfere. Suppose $\Delta\phi = \pi$. This corresponds to a shift of half of a wavelength between the two plane waves. With $\Delta\phi = \pi$, $A_2(\mathbf{x}, t) = Ae^{i(k\mathbf{x}-\omega t+\pi)} = e^{i\pi}A_1(\mathbf{x}, t) = -A_1(\mathbf{x}, t)$ so adding these two waves together will cancel one another out, resulting in a region containing a plane wave of amplitude 0. This is called destructive interference. On the other hand, if $\Delta\phi = 0$, then $A_1(\mathbf{x}, t) = A_2(\mathbf{x}, t)$ and adding the two waves together will result in a region containing a plane wave of amplitude $2A$. This is called constructive interference. When the phase shift is something other than 0 or π, the result will be a region containing an interference pattern

which arises due to the plane waves constructively interfering at some points and destructively interfering at other points.

2.1.2 Reflection

There are two main types of electromagnetic wave reflection: specular reflection and diffuse reflection [6]. A simple example of specular reflection would be light reflecting in a mirror. This occurs when light coming from one direction hits a smooth surface and is redirected in another single direction. Most surfaces however, reflect light diffusely. Diffuse reflection occurs when light coming from one direction hits a rough surface and is reflected in many different directions. Figure 2.2 gives a visual representation of the two types of reflection. An important difference between specular and diffuse reflection is that a smooth, flat surface that specularly reflects radiation can easily be angled in such a way that if a source emits radiation that is reflected off of the surface, then none of the reflected radiation will be reflected back towards the source. If the smooth, flat surface is instead replaced with a rough, flat surface that diffusely reflected light, then ensuring that none of the radiation is reflected back towards the source would be difficult or impossible to accomplish.

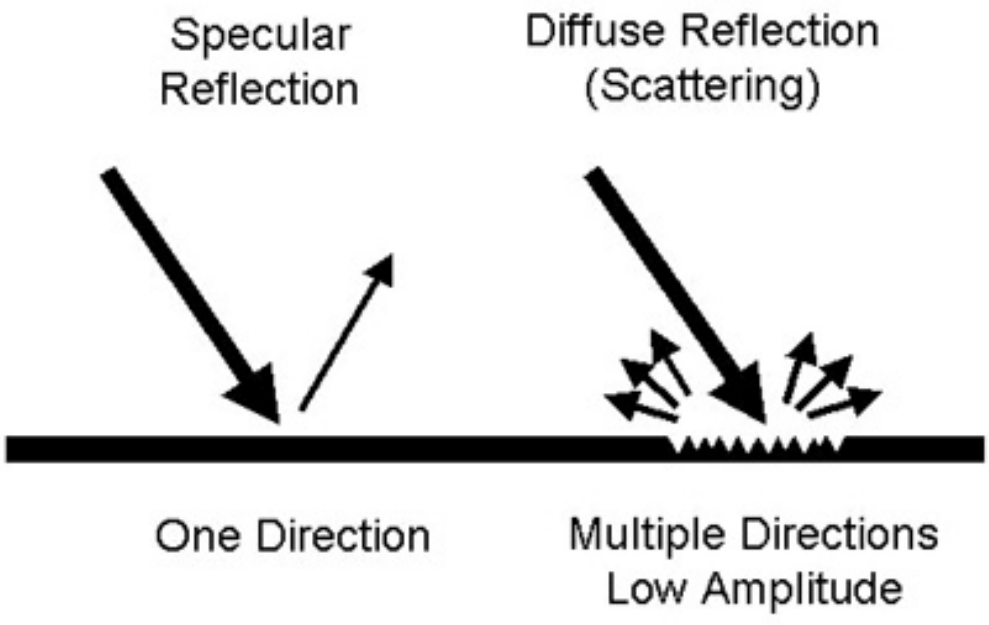

Figure 2.2: A side-by-side comparison of specular reflection and diffuse reflection [1].

2.2 Radars

Radar systems come in a wide variety of forms and are used for a diverse set of applications, but they all work on the same fundamental principles. A radar transmits a burst of radio waves or microwaves in a particular direction and listens for an echo. Figure 2.3 shows a diagram of a radar emitting radiation that bounces off the target. Based on the time between the emission of the radiation and the detection of the echo, the distance to the target can be calculated . The formula for this calculation is $r = \frac{ct}{2}$ where r is the range, t is the time between emission and detection of the echo and c is the speed of light. This distance, along with the direction in which the radar was pointing when it transmitted the burst, allows the location of a target to be determined. Additionally, the frequency of the radar has an impact on its performance. As the radar frequency increases, the resolution of the target also increases. The increase in resolution, however, comes at the

expense of higher atmospheric attenuation of the radar signal. As a result of this tradeoff, different frequencies are used depending on the demands of a particular situation.

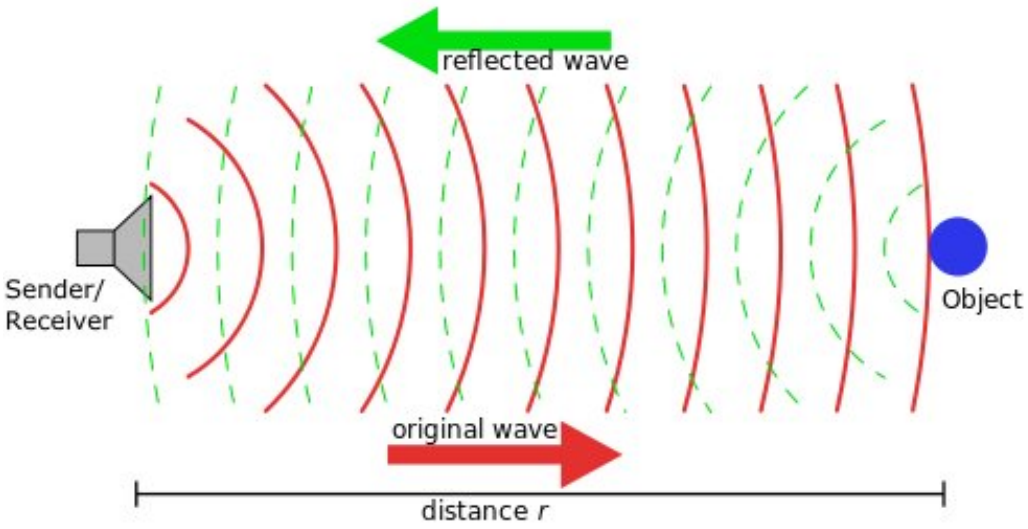

Figure 2.3: The distance to the target is half of the total distance that the radio waves from the radar have to travel [11].

The above explanation, however, is an idealized and oversimplified explanation of how a radar works. In reality, the radar will detect an echo from the target, but it will also pick-up general white noise which includes electronics noise as well as environmental noise. These noise signals can obscure or even mimic a target echo. An equation that is used for understanding how the radar detects what it does, and which is at the very core of understanding radar detection, is the radar range equation which calculates the signal to noise ratio (SNR). The formula for the SNR is [19, p. 66-67]

$$SNR = \frac{\sigma_s^2}{\sigma_n^2} = \frac{PG^2\lambda^2\sigma n_p^{f_p}}{(4\pi)^3 R^4 k T_0 F B L}. \tag{2.1}$$

where:

P is the peak power in Watts

G is the gain and equal to $\frac{4\pi A}{\lambda^2}$ (A is the effective area of the aperture)

λ is the operating wavelength of the radar in meters

σ is the radar cross-section (RCS) of the target which is discussed in more depth below.

n_p is the number of pulses used in each measurement

f_p is equal to 1 with coherent pulse integration and 0.7 otherwise (these values are based on observation [19, p. 67])

R is the range of the target in local spherical coordinates in meters

k is the Boltzman Constant, $1.38 \times 10^{-23} JK^{-1}$

T_0 is the noise temperature and assumed to be $290K$ in most cases

F is the noise figure which describes the general ambient white noise (but not clutter)

B is the bandwidth which is the inverse of the pulse width

L is the system loss which describes attenuation of the radar signal

σ_s^2 is the signal power or mean square voltage induced by the echo

σ_n^2 is the noise power or mean square voltage induced by the background noise.

The noise temperature, noise figure, and bandwidth along with Boltzmann's constant account for the noise that competes with the radar signal. The system loss accounts for the portion of the signal that is lost to atmospheric attenuation and internal resistance within the electronics. The radar range equation is therefore computing the ratio between the signal with the losses accounted for and the noise.

2.2.1 Radar Cross Section

The radar cross-section of a target—commonly referred to as RCS—can be understood as the cross-sectional area of a perfectly reflecting sphere that would produce a reflected signal equal in intensity to the one produced by the target. Although measured in square meters, the RCS should not be confused with a physical cross-section but instead should be thought of as an abstraction. The RCS of a target is highly dependent on physical orientation and can be much smaller than the physical cross-section of a target, as is the case with stealth aircrafts, or much greater, as can be the case with a rectangular flat plate [13]. More formally the RCS of a target is defined as

$$\sigma = \lim_{R \to \infty} 4\pi R^2 \frac{|E_s|^2}{|E_0|^2} \tag{2.2}$$

where: R is the distance to the target, E_0 is the incident electric field at distance R from the radar, and E_s is the electric field scattered back towards the radar at distance R from the radar. While Equation 2.2 will always define the RCS, the particular frequency or wavelength of the radiation used has a significant impact on the value of E_s for a particular object and is a direct consequence of the ideas covered in Section 2.1. Much like how particles scatter radiation based on the ratio between their circumference and the wavelength of the radiation, the target can be treated as a particle and therefore the dimensions of the target with respect to the wavelength of the incident radiation will affect the intensity of the signal that arrives back at the radar. If the true cross-section of an object is assumed to be a circle of radius r, then the wavelength affects the RCS behavior in three distinct regions as seen in Figure 2.4: when $\frac{2\pi r}{\lambda} \ll 1$, $\frac{2\pi r}{\lambda} \approx 1$ and $\frac{2\pi r}{\lambda} \gg 1$. When the circumference of the target is much less than the wavelength, i.e.$\frac{2\pi r}{\lambda} \ll 1$, the radar cross-section is proportional to $\left(\frac{r}{\lambda}\right)^4$ and will therefore tend to be much smaller than the true cross section [5]. This is known as the Rayleigh Region and in practice, it places a lower limit on the RCS of a target that a radar can detect because $\left(\frac{r}{\lambda}\right)^4$ rapidly converges to 0 as r decreases below λ. The Mie Region occurs when $\frac{2\pi r}{\lambda} \approx 1$ and is characterized by an oscillation in the RCS. The oscillating behavior is caused by the interference of the incident radio wave and creeping wave—the wave that diffracts around the target and travels back towards the radar—as the two waves move in and out of phase [20]. However, for most practical radar applications, the RCS falls into the Optical Region where $\frac{2\pi r}{\lambda} \gg 1$ and the oscillations from the Mie Region converge on the true cross-section of the target. RCS detection is therefore optimized when the operating wavelength of the radar is small compared to the dimensions of the target or in other words, the frequency is relatively high. It should be noted however, that past a certain point, further increases in the radar frequency will not improve the RCS and it fact will cause a decrease in the radar performance due to atmospheric attenuation, which will be discussed in the next subsection.

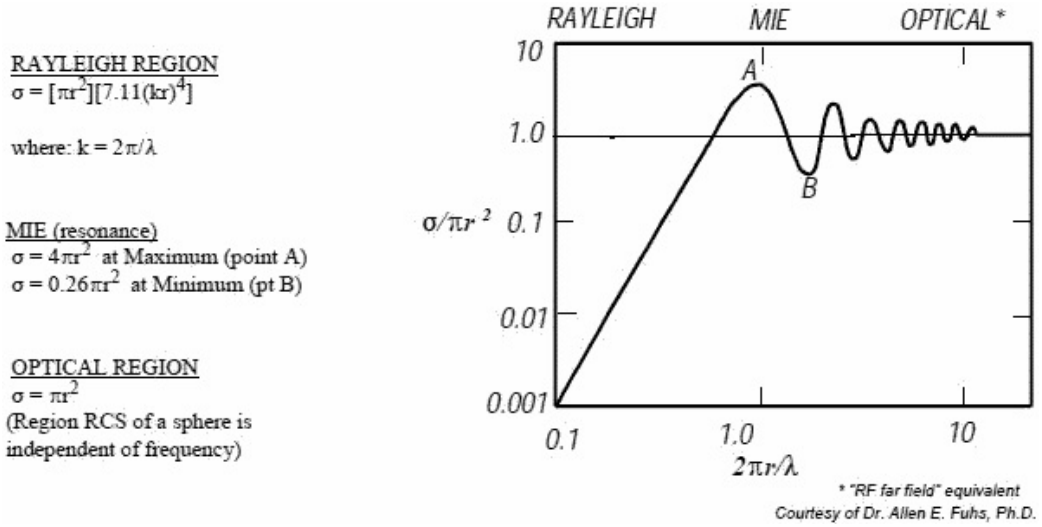

Figure 2.4: The ratio of RCS to the true cross-section as a function of the ratio of radius to wavelength has three distinct regions of behavior [2].

Stealth technology works by reducing the RCS that is visible in the direction of the radar. This is accomplished through a combination of customizing the shape of the body and the application of a radiation absorbing material [7]. The shape of the vehicle is designed to minimize the reflection of radiation back towards the radar. In Figure 2.5, the body of the stealth aircraft is comprised of many facets that intersect at sharp angles. The smooth angled facets ensure that as much of the incident radiation as possible is specularly reflected away from the radar's receiver. In addition to the shaping of the body, a layer of radiation absorbent material is added. The radar absorbent material—the most well known of which is iron ball paint—absorbs radiation in the radio spectrum and re-emits the energy as heat, which is invisible to radars [4]. The combinations of these two factors can reduce the radar signature of the aircraft to that of a small bird or large insect [18].

Figure 2.5: A frontal view of the Lockheed F-117 Nighthawk in flight [3].

2.2.2 Atmospheric Attenuation

The atmospheric attenuation of the radar signal is an important component in the system loss variable of Equation 2.1. The main contributors to this signal loss are atmospheric oxygen, O_2, and water vapor, H_2O [9]. RF wavelengths are absorbed by these two molecules and the energy is re-emitted as heat. In Figure 2.6, there is a general increase in signal attenuation as the frequency increases, but there are also several localized jumps. These jumps correspond to different resonant frequencies of the O_2 and H_2O molecules. As is evident in Figure 2.6, using a radar signal at one of the resonant frequencies can severely undermine the radar's performance. For example, if the operating frequency of the radar were set to 60 GHz, then for each kilometer that the signal travelled, the intensity would be reduced by 2-3 orders of magnitude.

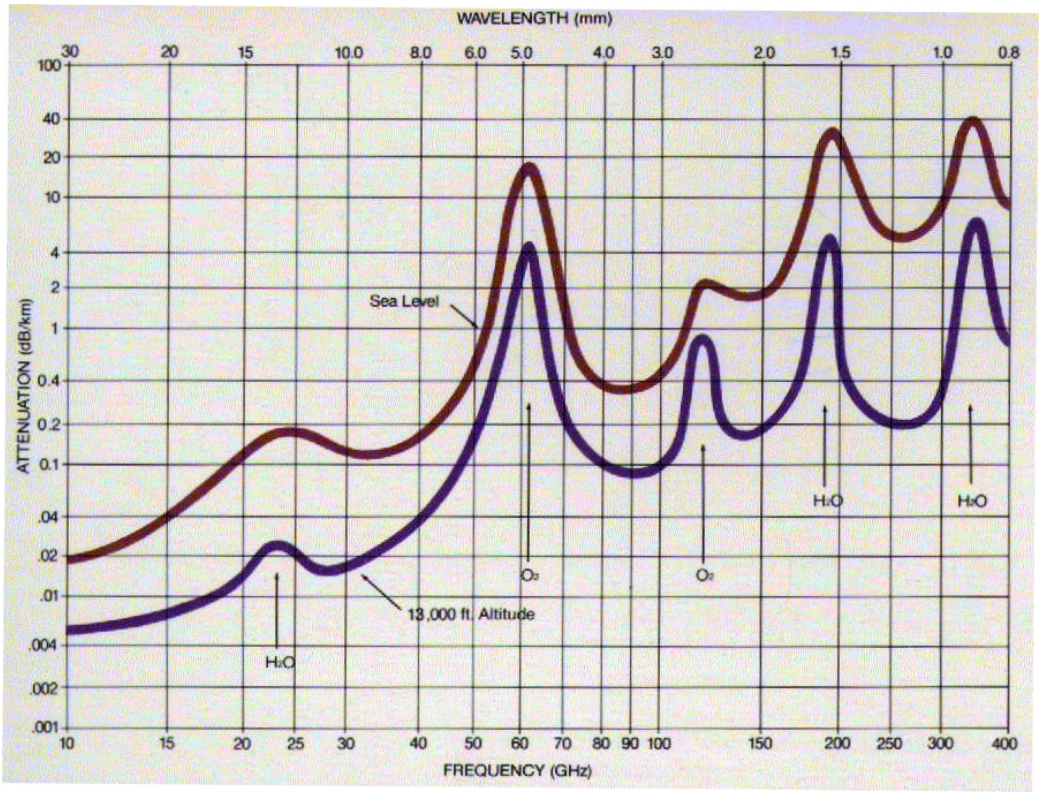

Figure 2.6: Atmospheric attenuation of RF waves as a function of frequency [12].

2.2.3 Detection

The SNR is not a value that the radar ever directly measures. The signal that the radar does detect is the combined noise and target echo signals. For most radar applications, there is a fluctuation of both the noise and echo signals. The signal that the radar observes is therefore the sum of two random variables—that is a quantity that can take on a value with a probability dictated by a probability density function— and as a result of this, it is not readily apparent whether or not a given spike in the measured signal is the result of a detection or is merely a random fluctuation. The noise signal is comprised of an in-phase vector component and quadrature vector component—both of which follow zero mean Gaussian distributions—

and therefore always follows a Rayleigh distribution [8]. The target echo signal, however, can follow one of several probability density distributions depending on the way in which the target scatters the incident radiation, or in other words, how the RCS of the target fluctuates as it moves with respect to the radar [21]. For aerial target applications, the RCS has a scan-to-scan fluctuation that follows a Gaussian probability density function (pdf), resulting in a measured echo signal that also fluctuates according to a Gaussian pdf [21]. This type of RCS fluctuation is described by the Swerling 1 model. As the measured signal is the sum of the Rayleigh distributed noise signal and Gaussian distributed echo signal, which are independent from one another, it too will be Rayleigh distributed. This simplifies the calculations as will become evident below.

As a fluctuating voltage amplitude is the only information that the radar operator has direct knowledge of, the method by which most of these fluctuations are filtered out is by setting a threshold voltage V_T below which a detection is not registered and which serves to limit false detections. The probability of a false alarm P_{FA} occurring with a particular threshold voltage setting can therefore be computed by taking the integral of the noise pdf over all voltages greater than the threshold voltage. This is given by [19, p. 99-108]

$$P_{FA} = \int_{V_T}^{\infty} p_n(v)\, dv = \int_{V_T}^{\infty} \frac{v}{\sigma_n^2} \exp\left(\frac{-v^2}{2\sigma_n^2}\right) dv = \exp\left(\frac{-V_T^2}{2\sigma_n^2}\right). \tag{2.3}$$

Solving for V_T in terms of P_{FA} defines a threshold voltage for an arbitrary false alarm probability as

$$V_T = \sqrt{2\sigma_n^2 \ln\left(\frac{1}{P_{FA}}\right)}. \tag{2.4}$$

Note that the false alarm probability must still be greater than 0 and less than or equal to 1, as the theshold voltage would otherwise have an imaginary—or at $P_{FA} = 0$, an infinte—value. To compute the actual probability of detection, the probability density function of the signal plus noise is integrated across all voltages greater than the threshold voltage. Because the combined echo plus noise signal has a Rayleigh distribution, the probability of detection can be calculated in the exact same manner as the probability of false alarm was for the noise signal.

$$P_D = \int_{V_T}^{\infty} p_{s+n}(v)\,dv = \int_{V_T}^{\infty} \frac{v}{\sigma_s^2+\sigma_n^2}\exp\left(\frac{-v^2}{2\left(\sigma_s^2+\sigma_n^2\right)}\right)\,dv$$
$$= \exp\left(\frac{-V_T^2}{2\left(\sigma_s^2+\sigma_n^2\right)}\right) \quad (2.5)$$

As $SNR = \frac{\sigma_s^2}{\sigma_n^2}$ by definition, some algebraic manipulation reveals that

$$P_D = \exp\left(\frac{-V_T^2}{2\left(\sigma_s^2+\sigma_n^2\right)}\right) = \exp\left(-\frac{\frac{V_T^2}{2\sigma_n^2}}{\frac{2(\sigma_s^2+\sigma_n^2)}{2\sigma_n^2}}\right) = \exp\left(-\frac{\ln\left(\frac{1}{P_{FA}}\right)}{\frac{\sigma_s^2}{\sigma_n^2}+1}\right)$$
$$= P_{FA}^{\frac{1}{1+SNR}} \quad (2.6)$$

or

$$SNR = \frac{\ln(P_{FA})}{\ln(P_D)} - 1 = -\left(\frac{2(\sigma_s^2+\sigma_n^2)\ln(P_{FA})}{V_T^2}+1\right) \quad (2.7)$$

This result allows the SNR to be computed using the measured signal, $\sigma_s^2+\sigma_n^2$; threshold voltage, V_T; and false alarm probability, P_{FA}. Additionally, the requisite SNR for an arbitrary false alarm probability and probability of detection can now be computed.

2.2.4 Measurement Uncertainty

With the SNR known, it is possible to determine the measurement uncertainties. The resulting effect of these uncertainties is that the measured flight path of the target will be noisy. For monopulse radars, the standard deviations of the estimated range, azimuth, and elevation values are respectively [19, p. 695][22]

$$\sigma_R = \frac{c}{2B\sqrt{2SNR}} \quad (2.8)$$

$$\sigma_\theta = \frac{\theta_{3dB}}{1.6\sqrt{2SNR}} \quad (2.9)$$

$$\sigma_\phi = \frac{\phi_{3dB}}{1.6\sqrt{2SNR}} \quad (2.10)$$

where:

c is the speed of light
B is the radar bandwidth
θ_{3dB} is the 3 decibel azimuthal beam width
ϕ_{3dB} is the 3 decibel elevational beam width

In addition to noise and the occasional false alarm, radars will typically pick up clutter which represents physical objects in the environment other than the target that is being tracked. Sources of clutter are wide ranging, from wind turbines to rush hour traffic; many things can produce unwanted radar signals that obfuscate the target echo.

2.2.5 Jamming

Radar jamming is when an adversary intentionally emits a signal that is intended to interfere with the radar's operation. While there are many different types of activities that may be referred to as jamming, the most common one is when radio transmissions are used to overwhelm the radar detector [10, p. 4-7.1]. When a jammer saturates a radar receiver with noise, the SNR is decreased which makes it difficult or impossible to make an accurate detection.

Various methods exist to counter radar jamming. One of the most effective countermeasures, however, is called frequency hopping, and it entails rapidly changing the operating frequency of the radar [16]. Radar jammers work by saturating a certain frequency band with noise and frequency hopping allows the radar to switch to a frequency not being jammed. As the power requirements for jamming the entire electromagnetic spectrum are prohibitive, frequency hopping is extremely difficult to counter.

2.3 Kalman Filter

Unprocessed radar measurement data contains a significant quantity of undesired noise, false alarms and clutter. The Kalman filter is a powerful mathematical tool that makes it possible to remove much of these unwanted signals and has the effect of reducing positional uncertainty, thus producing a more accurate estimation of the true position of the target than the unprocessed radar measurements alone. In a general sense, the Kalman filter works by taking a weighted average of the measured state of the target (position, velocity, and acceleration) and a predicted value of the state of the target that is based off of previous measurements. The factor that is responsible for this weighting between the measured and predicted values is called the Kalman gain and will be discussed below.

For all of the subscripts in this section that include two values separated by a vertical line, the first number in the subscript refers to the number time step being computed and the second number refers to the time step up until which we are using to make this computation. For example $\hat{\mathbf{x}}_{k|k-1}$ can be read as the computed value of the state vector at time step k using all of the measurements up to and including time step k-1. In contrast, $\hat{\mathbf{x}}_{k|k}$ is the state vector at time step k using all of the measurement up to and including time step k. More simply stated, $\hat{\mathbf{x}}_{k|k-1}$ is the predicted state vector at time step k whereas $\hat{\mathbf{x}}_{k|k}$ is the true state vector at time step k. The subscripts that only include a single value represent the value of the parameter at that time step.

The Kalman filter is implemented via a recursive algorithm and outputs a state vector (position, velocity, and acceleration) and covariance matrix (position, velocity and acceleration uncertainty) for each time step. The Kalman filter is initially seeded with an unprocessed state vector $\hat{\mathbf{x}}_{0|0}$ and covariance matrix $P_{0|0}$. A prediction for the state vector and covariance matrix is then made for the next time step based on the previous time step. For an arbitrary timestep k, the predictions at time step k will be calculated from the values of state vector and covariance matrix estimates from time step k-1 (or the initial seeded values when $k = 1$) such that [17]

$$\hat{\mathbf{x}}_{k|k-1} = F_k \hat{\mathbf{x}}_{k-1|k-1} + B_k \mathbf{u}_k \tag{2.11}$$

$$P_{k|k-1} = F_k P_{k-1|k-1} F_k^T + Q_k \tag{2.12}$$

where:

F is the state transition matrix $F = \begin{bmatrix} 1 & \Delta t & \frac{\Delta t^2}{2} \\ 0 & 1 & \Delta t \\ 0 & 0 & 1 \end{bmatrix}$

B is the input control transition matrix (assumed to be zero here)

$\mathbf{u}$ is the input control vector (assumed to be zero here)

Q is the process noise covariance.

The state transition matrix serves to change the state as a function of time. In the case here of a target in motion, the state transition matrix takes on the form of the standard kinematics equation. The control commands and control vector pertain to the amount of physical control that one has over the motion of the target. As the radar is merely observing the target, both of these values are set to 0. The process noise covariance is the term that accounts for any physical perturbations in the motion of the target.

The prediction is updated by taking a weighted average between the predicted and measured valued at the k^{th} time step [17].

$$K_k = P_{k|k-1} {H_k}^T \left(H_k P_{k|k-1} {H_k}^T + R_k \right)^{-1} \tag{2.13}$$

$$\hat{\mathbf{x}}_{k|k} = \hat{\mathbf{x}}_{k|k-1} + K_k \left(\mathbf{z}_k - H_k \hat{\mathbf{x}}_{k|k-1} \right) \tag{2.14}$$

$$P_{k|k} = (I - K_k H_k) P_{k|k-1} \tag{2.15}$$

where:

R is the measurement error covariance matrix

K is the Kalman gain or the weighting factor

$\mathbf{z}$ is the observed state vector

H is the measurement matrix.

The measurement error covariance is the term that contributes to the uncertainty in the state of the target. Accurately accounting for the measurement covariance is one of the main objectives of the Kalman filter. The Kalman gain is the term that determines the weighting in the weighted average of the observed and predicted states. The observed state vector is the state value of the target that the radar measures. The measurement matrix maps the true state vector of the target, $\mathbf{x}$, into the observed state vector.

These equations are applied to every time step and the result is a more accurate representation of the true position of the target.

Chapter 3

Methodology

3.1 Radar Simulator

The radar simulation tool was built to simulate radar measurements for the tracker. The simulated environment consisted of a system of one or more radars and a single target. The simulator was given input data for the target and radar. The target inputs were the waypoints of the target trajectory— which are coordinates that define the path of the target flight— in geodetic coordinates (latitude, longitude, altitude), the timestamps that corresponded to each waypoint and the target RCS. The number of radars could be arbitrarily set, but for each individual radar, the inputs were: the radar location in geodetic coordinates; radar aperture type which could be a parabolic antenna, linear array or a rectangular array; the effective area of the radar antenna; peak transmission power; operating frequency; noise figure; system loss; pulse width; the number of pulses used for each radar measurement; and whether or not the pulses were coherently integrated. The outputs of the simulation the coordinates of the locations along with the corresponding timestamps where the radar detected a target. This included both true detections and false alarms.

Figure 3.1 shows a screenshot of the radar simulation GUI after a run. The map on the left is generated using the outputs of the simulation. The small "x" markers represent the physical location of each radar. Each point on the map represents a detection with the color corresponding to the radar of the matching color which made that detection. The clustering of points that form the vertical line down the middle of the map are due to the target

and the points scattered all over the map are false detections. However, determining exactly which points correspond to the target(s), as opposed to those points representing a false detection, is one of the main purposes of the tracker and fuser.

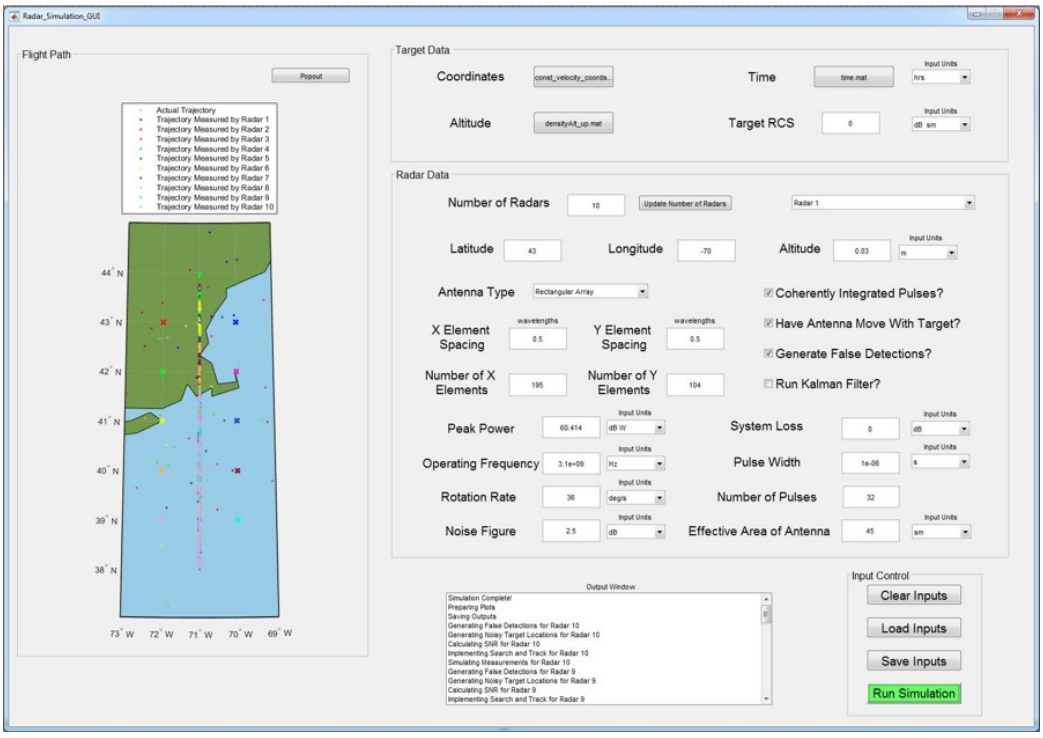

Figure 3.1: Radar simulation screenshot

The radar simulator ran a separate simulation for each one of the radars using the inputs for that specific radar. The first step in the simulation was to compute the SNR using Equation 2.1. The SNR was multiplied by an additional gain factor depending on which antenna type was selected. The additional gain accounts for the fact that the radar does not emit radiation isotropically but rather that the directionality of the radiation that the radar emits is dependent on the geometry of the radar aperture. This gain factor is different for each of the three apertures but is always a function of the target elevation and azimuth relative to the center of the radar beam. The

gain factor for the parabolic antenna is

$$G_p = \left[\frac{J_1(kr\sin(\phi))}{kr\sin(\phi)}\right]^2 \tag{3.1}$$

where:

J_1 is the Bessel function of the first kind of order 1

k is the wavenumber

ϕ is the target elevation relative to the center of the radar beam (See Figure 3.2).

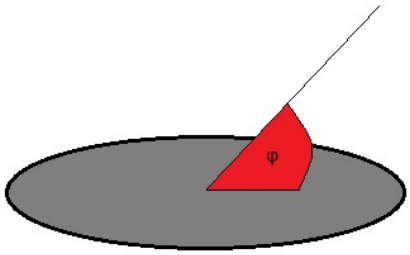

Figure 3.2: Diagram of circular antenna

The linear array is assumed to be comprised of N isotropically emitting elements with uniform spacing between them. The gain factor for the linear array is

$$G_l = \left[\frac{1}{N}\frac{\sin\left(\frac{Nkd\sin(\phi)}{2}\right)}{\sin\left(\frac{kd\sin(\phi)}{2}\right)}\right]^2 \tag{3.2}$$

where:

N is the number of elements in the array

d is the spacing between elements

k is the wavenumber and is equal to $\frac{2\pi}{\lambda}$ where λ is the radar operating wavelength

ϕ is the target azimuth relative to the center of the radar beam (See Figure 3.3).

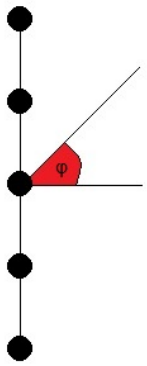

Figure 3.3: Diagram of linear array aperture

The rectangular array is treated as two perpendicularly arranged linear arrays with M isotropically emitting elements along one and N isotropically emitting elements along the other. The gain factor for the rectangular array is

$$G_r = \left[\left| \frac{\sin\left(\frac{Mkd\sin(\theta)\cos(\phi)}{2}\right)}{M\sin\left(\frac{kd\sin(\theta)\cos(\phi)}{2}\right)} \right| \left| \frac{\sin\left(\frac{Nkd\sin(\theta)\sin(\phi)}{2}\right)}{N\sin\left(\frac{kd\sin(\theta)\sin(\phi)}{2}\right)} \right| \right]^2 \tag{3.3}$$

where:

M is the number of elements in the array along the x direction

N is the number of elements in the array along the y direction

d is the spacing between elements in the array

k is the wavenumber and is equal to $\frac{2\pi}{\lambda}$ where λ is the radar operating wavelength

θ is the target azimuth relative to the center of the radar beam (See Figure 3.4)

ϕ is the target elevation relative to the center of the radar beam (See Figure 3.4).

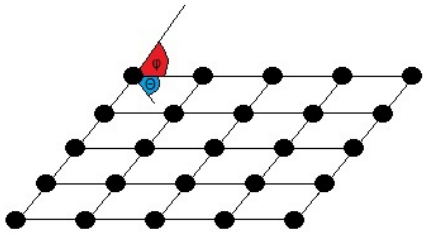

Figure 3.4: Diagram of rectangular array aperture

The antenna/aperture gain was incorporated into the simulation by multiplying the SNR by the antenna/aperture gain factor. An additional constraint on the SNR that has not yet been detailed is the horizon. Electromagnetic radiation travels in a straight line and so any target below the horizon will not be detected (we assumed no atmospheric reflection in the simulation). The radar range equation multiplied with the aperture/antenna gain factor allowed the simulator to assign an SNR to the target at every time step based on the distance between the radar and the target. To account for the effects of the horizon, a conditional statement was added into the

simulator that set the SNR of the target to 0 if the distance between the target and radar exceeded the distance from which the target was above the horizon with respect to the radar. The equation for the greatest distance at which the radar could observe the target is

$$d_{max} = \sqrt{2R_E h_{rdr}} + \sqrt{2R_E h_{tgt}} \tag{3.4}$$

where:

h_{rdr} is the altitude of the radar

h_{tgt} is the altitude of the target and is equal to $R\sin(El)$ when expressed in spherical coordinates with the radar at the origin

R_E is the mean radius of the Earth.

After the SNR was computed for the target at every time step, the next step was to compute a probability of detection based off of the SNR at each of those time steps. The simulation used a Swerling 1 probability density function which was defined as

$$P_D = \begin{cases} \exp\left(-\frac{\nu_t}{1+SNR}\right), & \text{if } n_p = 1 \\ 1 - \Gamma_1(\nu_t, n_p - 1) + \left(1 + \frac{1}{n_p SNR}\right)^{n_p - 1} \Gamma_1(\frac{\nu_t}{1+\frac{1}{n_p SNR}}, n_p - 1), & \text{if } n_p > 1 \end{cases} \tag{3.5}$$

where:

ν_t is the threshold value

Γ_1 is the incomplete gamma function

n_p is the number of pulses.

A random number generator produced a value between 0 and 1 for every time step. If the value was less than or equal to the decimal representation of the computed probability of detection at the time step, the target was determined to have been detected, otherwise the target was not detected. The final part of the radar measurement simulation was to generate the coordinates where the radar detected the target. When measuring radar positions, there is an SNR related error associated with the target range, elevation, and azimuth. As the exact trajectory of the target is known in the radar simulation tool (because it was one of the input values), the detected positions of the target are simulated by taking the exact positions and offsetting those positions by a random displacement value taken from a normal distribution

number generator using the standard deviations calculated in Equations 2.8-2.10.

Included in the radar simulator was an option to add false alarms to the simulated measurements. The default false alarm probability was 10^{-6} and the number of range bins was 2000 for each time step. That equated to each range bin having a 10^{-6} probability of triggering a false alarm. The false alarms were mixed in with the true detection before the results of the simulation were outputted.

Clutter is an important factor in radar tracking and so it was necessary to incorporate some form of it in the simulation to see how the tracker would process it. As clutter is physically representative of various objects of non-interest in the environment, the occurrence of clutter detections should not fit neatly into some Gaussian or uniform distribution over the entire simulated environment. Instead, it was decided that the most straightforward approach would be to generate regions of various sizes all throughout the environment and have a probability of detecting a scattered object at every point in each region. Through this approach, all of the detections caused by a scattered object would be localized to these regions and the rest of the environment that existed outside of the regions would have no scatter-caused detections at all. The region based approach to incorporating clutter has it's drawbacks, namely that clutter objects should still be following clearly defined trajectories, but the idea was that the algorithm would still try to make sense of these anomalous albeit localized detections by either incorporating them into a new track or filtering them out.

3.2 Tracker

The radar simulator included an additional option to apply a tracking algorithm to the outputs and form tracks. Much of the tracker code already existed and was simply incorporated into the radar simulator. The tracker utilized Equations 2.11 through 2.15. The basic tracker algorithm is shown in Figure 3.5.

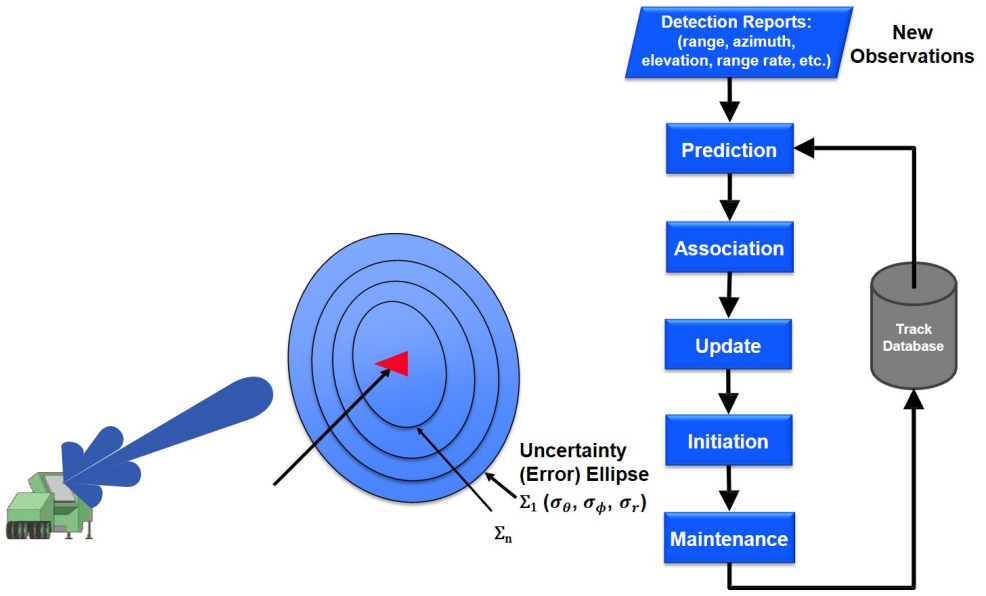

Figure 3.5: The algorithm for the target tracker [14].

The tracker began by taking one of the radar measurements. Using Equations 2.11 and 2.12, a prediction for the target's next location was made. If there was a subsequent measurement in the vicinity of the prediction, that measurement and the previous measurement used to make the prediction would be associated together as being from the same target. Equations 2.14 and 2.15 were then used to update the prediction using the new measurement. If however, there was not a subsequent measurement in the vicinity of the prediction, a new track would be initiated. The final step was to discontinue any tracks that failed to get associated with a new measurement for five consecutive time steps. This algorithm would then repeat itself until all measurements were grouped into tracks.

3.3 Track Quality

Determining which factors make one track of a higher quality than another track is somewhat of a challenge. Depending on the situation, the length of a track, accuracy of a track, or total coverage of all tracks may be deemed the highest priority. Due to the controlled nature of the simulation,

there is perfect knowledge of the system and this can be used to construct any number of different metrics to determine the quality of a track. The metric that was used as the basis for the comparison in this paper is a combination of the length of the longest continuous track and the median error between the points in the longest track versus the points where the target actually was at those time steps.

Chapter 4

Conclusion and Discussion

While the fusion simulations were accurate enough to compare the fusion algorithms in simple scenarios, the limitations of the simulation program became evident when we proceeded beyond simple flight trajectories. One element that proved difficult to incorporate into the radar simulator was clutter, meaning detections that are caused by an object of non-interest. The presence of clutter and other unwanted background noise was accounted for by increasing the false alarm rate on the radar simulators but this was a compromise that was made when a clutter model proved too difficult to implement. A more realistic model of clutter should be included in the future.

Additionally, the tracking on the setups with the maneuvering target(s) was far more optimal that what should have been observed. This was likely due to the fact that the radar simulator did not incorporate Doppler velocity which would have added additional uncertainty in the radial direction measurements. What instead happened was that as the target maneuvered back and forth radially, it remained in the radar's field of view for longer, resulting in more measurements and, without the additional uncertainty, that produced more accurate tracks. A more realistic radar simulator would incorporate the Doppler velocity and could expand upon this work.

Bibliography

[1] Echo reflection and scattering. [Online; accessed Fedbruary 2016].

[2] Electronic warfare and radar systems engineering handbook - radar cross section (rcs) - rf cafe. [Online; accessed Fedbruary 2016].

[3] F-117 nighthawk front - stealth aircraft - wikipedia, the free encyclopedia. [Online; accessed Fedbruary 2016].

[4] Radar absorbing materials information — ihs engineering360. [Online; accessed Fedbruary 2016].

[5] Radar cross section. [Online; accessed Fedbruary 2016].

[6] Reflection of light, April 2012. [Online; accessed Fedbruary 2016].

[7] William F Bahret. The beginnings of stealth technology. *IEEE Transactions on Aerospace and Electronic Systems*, 29(4):1377–1385, 1993.

[8] David Knox Barton. *Radar system analysis*. Artech, 1976.

[9] Federal Communications Commission et al. Millimeter wave propagation: spectrum management implications. *Bulletin*, 70, 1997.

[10] NAVAIR Avionics Department. *Electronic Warfare and Radar Systems*. Naval Air Warfare Center Weapons Division, fourth edition, October 2013.

[11] Dragos Calin. Types of sensors for target detection and tracking, 2013. [Online; accessed November 2015].

[12] Ramesh Gavva. Satellite communications seminar report — 1000 projects. [Online; accessed Fedbruary 2016].

[13] Doren W Hess. Introduction to rcs measurements. In *Antennas and Propagation Conference, 2008. LAPC 2008. Loughborough*, pages 37–44. IEEE, 2008.

[14] Lincoln Laboratory. Target tracker diagram. Personal communication.

[15] Marc Leger. Why the sun can harm you and wifi cant (and how microwave ovens cook your food), 2013. [Online; accessed Fedbruary 2016].

[16] Sami A Mostafa. Frequency hopping transceiver system with application to radar.

[17] Ian Reid. Estimation ii. *Tutorial, University of Oxford*, 2001.

[18] Mirabel Cerqueira Rezende, Inácio Malmonge Martin, Roselena Faez, Marcelo Alexandre Souza Miacci, and Evandro Luus Nohara. Radar cross section measurements (8-12 ghz) of magnetic and dielectric microwave absorbing thin sheets. *Revista de Fısica Aplicada e Instrumentaçao*, 15(1), 2002.

[19] Mark A Richards, Jim Scheer, and William A Holm. *Principles of Modern Radar: Basic Principles*. SciTech Pub., 2010.

[20] Merrill Skolnik. *Radar Handbook Second Edition*. McGraw-Hill, New York, 1990.

[21] Peter Swerling. Probability of detection for fluctuating targets. *Information Theory, IRE Transactions on*, 6(2):269–308, 1960.

[22] Ryuhei Takahashi, Kazufumi Hirata, Teruyuki Hara, and Atsushi Okamura. Derivation of monopulse angle accuracy for phased array radar to achieve cramer-rao lower bound. In *Acoustics, Speech and Signal Processing (ICASSP), 2012 IEEE International Conference on*, pages 2569–2572. IEEE, 2012.